scientific reports

Check for updates

OPEN

In situ forming gels as subcutaneous delivery systems of curcumin and piperine

Walter Pula[1], Alessia Pepe[2], Francesca Ferrara[1], Agnese Bondi[1], Paolo Mariani[2], Maria Grazia Ortore[2], Alessandra Pecorelli[3,4], John Ivarsson[5], Giuseppe Valacchi[3,5,6]✉ & Elisabetta Esposito[1]✉

In this study an in situ forming gel for curcumin and piperine delivery is investigated as a long-lasting strategy in the local treatment of inflammatory and degenerative joint disease, such as osteoarthritis and rheumatoid arthritis. Particularly glyceryl monooleate, in association with phosphatidylcholine and ethanol, were employed. Different ratios between excipients were tested, with the aim to obtain a liquid form suitable for subcutaneous injection, gaining a semisolid consistency in contact with biological fluids. A formulative study was conducted to assess the composition impact on the structural properties of the formulations, particularly focusing on injectability and phase transition. Curcumin and piperine were loaded, singularly or jointly, in selected in situ forming gels. Structural characterization, performed by X-ray scattering, revealed disordered reverse micellar phases, undergoing transition to hexagonal and cubic *Pn3m* phase upon hydration. In vitro dialysis release study demonstrated a sustained release of both drugs over 96 h, with a faster release in the case of jointly loaded drugs. Mechanistic analysis and water uptake studies indicated a drug release governed by both diffusion and swelling/erosion of the lipid supramolecular structure. Furthermore, an ex vivo release analysis performed using human skin explants suggested the formulation suitability for subcutaneous injection, indicating that the presence of piperine in the in situ formed gel allowed to double the curcumin release with respect to the simple curcumin loaded gel.

Keywords Glyceryl Monooleate, Skin, Hexagonal phase, Curcumin, Piperine

Several degenerative and inflammatory joint diseases affect patients around the world, leading to severe long-term pain and disability. Particularly, osteoarthritis (OA) is the main degenerative joint disease of the movable joints leading to localized loss of cartilage, adjacent bone remodelling, and overgrowth of bony. OA affected people suffers for joint pain, swelling, and are impaired by limited range of-motion with consequent compromised physical function and life quality. Ankylosing spondylitis, rheumatoid arthritis (RA), and gouty arthritis are the most common inflammatory joint diseases[1–3]. Among them, RA is a multifactorial, immune-mediated inflammatory disease afflicting up to 1% of the global adult population[4,5]. It is characterized by chronic synovial inflammation and hyperplasia, leading to erosive joint damage, functional impairment, and disability[6–9]. Over the past decades, due to a better understanding of OA and RA pathophysiology, the number of therapeutic resources available for the treatment of these diseases has grown significantly[10,11]. The current standard therapeutical treatment of OA and RA involves systemic administration of non-steroidal anti-inflammatory drugs, glucocorticoids, and disease-modifying anti-rheumatic drugs[12–14]. However, there have been increasing concerns regarding drug safety and efficacy profile. The percentage of treatment failure, including nonresponse and limited efficacy, is still significant, moreover the long-term use of the above reported drugs causes adverse clinical effects, such as gastrointestinal damage, cardiovascular adverse effects (i.e., aggravation of hypertension and/or heart failure, and an increased risk of thrombotic events), osteoporosis, infections, and

[1]Department of Chemical, Pharmaceutical and Agricultural Sciences, University of Ferrara, I-44121 Ferrara, Italy. [2]Department of Life and Environmental Sciences, Marche Polytechnic University, I-60131 Ancona, Italy. [3]Department of Environmental and Prevention Sciences, University of Ferrara, I-44121 Ferrara, Italy. [4]Plants for Human Health Institute, Department of Food, Bioprocessing and Nutrition Sciences, NC State University, NC Research Campus, 28081 Kannapolis, NC, USA. [5]Plants for Human Health Institute, Animal Science Department, NC State University, NC Research Campus, Kannapolis, NC 28081, USA. [6]Department of Food and Nutrition, Kyung Hee University, Seoul, South Korea. ✉email: vlcgpp@unife.it; ese@unife.it

kidney diseases[15–17]. Therefore, there is an urgent need to explore alternative and coadjutant treatments for managing OA, RA and other joint diseases.

In this regard, phytocompounds such as curcumin (CUR) and piperine (PIP), may represent a valuable therapeutic option or adjuvant strategy in the treatment of OA and RA, due to their low toxicity, pharmacological safety, and pharmacological activities. CUR and curcuminoid in general, are bioactive polyphenols from Turmeric (*Curcuma longa*) and have been shown to possess therapeutical properties, including antioxidant, antimicrobial, anti-neoplastic, and wound healing properties[18–20]. Moreover, CUR anti-inflammatory and immunomodulatory properties result in proven positive effects in the management of immune-mediated inflammatory disease, including OA and RA[21–24]. PIP, the major bioactive compound from *Piper nigrum*, is an alkaloid possessing a broad spectrum of pharmaceutical activities including antioxidant, anti-diabetic, anti-obesity, analgesic, antibacterial, hepato-protective, and neuro-protective properties[25,26]. Similarly to CUR, PIP also possesses anti-arthritic effects associated with its anti-inflammatory and immunomodulatory activities[27,28]. In addition, PIP is a recognized bio-enhancer able to increase the bioavailability of co-administered drugs through a complex and still not understood combination of different mechanisms[26,29]. Several studies have demonstrated that PIP significantly enhances CUR's bioavailability and activity by modulating its intestinal absorption and metabolism, as well as by acting as a penetration enhancer when co-administered topically[26,30–32]. Nevertheless, both CUR and PIP administrations are strongly limited by their poor solubility and low bioavailability, requiring specialized delivery strategies to overcome these limitations[33,34].

The local administration of drugs exploited by intra-articular injections represents an alternative strategy to the oral route in the treatment of OA and RA, offering the possibility to (i) precisely dose the active molecule directly to the lesion area, (ii) reduce toxic effect due to minimization of systemic distribution and (iii) enhance the bioavailability, avoiding hepatic first pass[35]. Nonetheless, intra-articular injections usually do not lead to stable effect, since simple solutions of drugs directly injected into the articular cavity are generally quickly cleared, due to enzyme degradation or cellular uptake. In this regard, recently, nanocarriers and scaffold materials have been developed[36]. Namely, lipid or polymeric based nanocarriers, microneedles, pre-formed solid implants, and injectable hydrogels, represent innovative strategies suitable to precisely modulate drug administration, controlling its release and distribution at the local site, while minimizing its degradation.

In this respect, in the present study an in situ forming gel (ISFG) based on lyotropic liquid crystal was developed to deliver CUR and PIP. The designed ISFG is composed of glyceryl monooleate (GMO) and phosphatidylcholine (PC) and has been optimized for subcutaneous co-administration of CUR and PIP in the treatment of RA. GMO is a biocompatible and biodegradable unsaturated monoglyceride classified as GRAS (generally recognized as safe) and included in the FDA Inactive Ingredients Guide[37]. The peculiar amphiphilic structure enables GMO to self-assemble in the presence of water into a range of thermodynamically stable liquid crystalline structures, depending on concentration, water content, temperature, and the presence of additives, such as PC, a zwitterionic surfactant that also spontaneously alters its supramolecular organization in the presence of water[38,39]. GMO-based ISFGs have emerged as a promising delivery technology for long-acting treatments, being characterized by high biocompatibility, biodegradability, and the capability to undergo sol-gel transition post-injection upon water absorption. The change of physical state, due to phase transition in contact with biological fluids, leads to semi-solid depot system able to sustain the release of the entrapped drugs[40]. In addition, phase transition should sustain the drug release from the ISFG precursor, avoiding possible toxic effects related to immediate drug release achieved by direct injection of simple drug solution, resulting in high drug concentration in the blood stream[41].

Several recent studies have demonstrated the advantages offered by the subcutaneous or intra-articular administration of standard anti-arthritic drugs, such as methotrexate and indomethacin, using injectable ISFG over conventional oral dosage forms[42–44]. Indeed, they can be easily formulated, sterilized, and administered topically or at specific sites within the body, reducing dosing frequency and improving patient compliance, while addressing challenges associated with oral administration, such as variable absorption[42,44]. In the present investigation, a formulative study was conducted to obtain a dosage form for CUR and PIP local delivery. The formulation had to be low viscous to be easily injectable subcutaneously, afterwards it should become semisolid in contact with physiological fluids. Structural characterization of both the unloaded and loaded ISFGs was performed using synchrotron Small Angle X-ray Scattering (SAXS) and X-ray Diffraction (XRD), while in vitro release study was conducted via the dialysis method. In addition, an ex vivo release analysis was performed using human skin explants.

Materials and methods

Materials

Curcumin ((E, E)−1,7-bis(4-Hydroxy-3-methoxyphenyl)−1,6-heptadiene-3,5-dione, purity grade 94%, CUR) and piperine (1-piperoylpiperidine, purity grade 97%, PIP) were purchased from Merck Life Science S.r.l. (Milan, Italy). Glyceryl monooleate (purity grade 94%) was purchased from Atam Chemicals (Istanbul, Turkey) and the soybean lecithin PC (purity grade 94%) was Epikuron 200 from Lucas Meyer (Hamburg, Germany). Solvents were of an HPLC grade, and all other chemicals were of an analytical grade.

Preparation of ISFG

The ISFG formulations were prepared by mixing dry GMO and PC at different GMO: PC ratios (8:2, 7:3, 6:4 and 5:5 w/w). Ethanol (50, 100, 150, 200 or 250 µL/g of final formulation) was then added to the resulting lipid matrix under magnetic stirring (IKA RCT basic, IKA®-Werke GmbH and Co., KG, Staufen, Germany) maintaining the temperature at 45 °C in a thermostatically controlled water bath, until obtaining a homogeneous mixture. In the case of CUR, PIP or CUR + PIP loaded formulations, CUR (1% w/w), PIP (1% w/w) or CUR + PIP (0.5% and 0.5% w/w) have been added to the samples after the addition of ethanol.

Syringeability and gelation test

The syringeability of the precursors was manually tested 24 h after preparation using 1 mL plastic syringe (MTD, plunger diameter 2 mm) equipped with a 26-G needle. In order to visually confirm the liquid-to-semisolid state transition of the precursor in presence of water, a preliminary gelation test was performed by injecting 500 µL of precursors into 5 mL of bidistilled water.

X-ray scattering study

Small Angle X-ray Scattering (SAXS) experiments were performed at the Austrian beamline in Elettra synchrotron located in Trieste (Italy)[45]. Samples were prepared in 2 mm diameter polycarbonate capillaries thermostated within a KPR (Peltier heating/cooling) sample holder (Anton Paar, Graz, Austria) at 37 °C. The exposition time for each sample was 1 min and 10 frames were collected for each of them. Two-dimensional (2D) data were corrected for background, detector efficiency, sample transmission and then radially averaged to derive the differential scattering cross-section, more simply scattered intensity *I*, as a function of the modulus of the scattering vector, *Q*, defined as $4\pi \sin\theta/\lambda$ (where 2θ is the scattering angle and λ the X-ray wavelength). The Q-range explored was between 0.01 and 0.5 $Å^{-1}$. The detector used for the measurement was a 2D Pilatus3 1 M Detector System with a pixel size of 172×172 μm^2 and a discrete energy of 8 keV (corresponding to the beam wavelength of 0.154 nm). An additional Wide-Angle X-ray Scattering (WAXS) detector was used to simultaneously monitor diffraction patterns in the high-angle range from 0.8 to 1.7 $Å^{-1}$. SAXS measurements were carried out on pre-hydrated samples.

X-ray Diffraction (XRD) experiments were performed using the Rigaku Smartlab diffractometer located at the Department of Science and Engineering of Matter, Environment and Urban Planning (SIMAU) of the Marche Polytechnic University (Ancona, Italy). The diffractometer has a rotating anode X-ray source of 9KW and operates at $\lambda = 1.54$ Å in the Bragg-Brentano configuration. The samples were placed in a sandwich holder thermostated at 37 °C at a distance from the 2D HPAD detector of 300 mm to explore a *Q*-range between 0.05 and 0.25 $Å^{-1}$. One frame was collected at 37 °C for each sample, using an exposition time of 5 min. Samples were prepared at different water compositions, c_w, defined by the ratio $C_{wat}/(C_{wat}+C_{ISFG})$ where C_{wat} and C_{ISFG} are the weight of water and ISFG components. respectively. XRD experiments were performed on samples whose c_w was 0.3, 0.4, 0.5; and the salt sample was prepared in excess of water (exc wat).

In vitro drug release study

The in vitro release of PIP and/or CUR from the selected ISFG formulations was determined by dialysis method. Briefly, 300 µg of ISFG loaded with CUR and PIP separately or jointly (10 mg/mL) were injected into the dialysis tube (Pur-A-Lyzer™ Maxi Dialysis Tube 0.1–3 mL, MWCO, 6–8 kDa, Merck, Milan, Italy), previously filled with 1 mL of bidistilled water (0.3 v/v vehicle/water ratio). The dialysis tube was then placed into 200 mL of receiving phase constituted of water/ethanol (50:50, *v/v*), maintained under constant magnetic stirring at 37 ± 1 °C. In addition, to evaluate the release kinetics of free PIP and CUR, 300 µL of CUR or PIP 10 mg/mL ethanol solution were injected in dialysis tubes, using the same equipment and condition adopted in the case of ISFG analysis. At predetermined time intervals between 1 and 96 h, samples (1 mL) of the receiving phase were collected and analyzed by HPLC as reported below to evaluate the CUR and/or PIP content. Each withdrawn sample was replaced with an equal volume of fresh receiving phase. PIP and CUR released amounts at each predetermined time were provided in six independent experiments, calculating the mean values ± s.d. The cumulative percentage of drug released with respect to the total amount of drug loaded in the formulation was plotted against the time to obtain the release profile. To gain insight into the release mechanism, the fitting of the experimental release data was analyzed using different mathematical release models: zero-order kinetics (cumulative % drug released vs. time), first-order kinetics (log cumulative % drug remaining vs. time), Higuchi (cumulative % drug released vs. square root of time), and Peppas (log cumulative % drug released vs. log time) models. The suitability of the model fits was verified using the DDsolver add-in for Excel 2016 (Version 2312 Build 16.0.17126.20126), using the correlation coefficient (R^2) as indicator of the best fitting, for each of the considered models. Furthermore, the Peppas model was employed to assess and characterize the influence of swelling and/or erosion phenomena on drug release. Specifically, the Ritger-Peppas, Korsmeyer-Peppas, or simply Peppas model (commonly referred to as the power law) is a semi-empirical model that establishes a straightforward exponential relationship between release and time, capable of considering and describing both diffusional and non-diffusional drug release processes[46]:

$$\frac{M_t}{M_8} = Kt^n$$

where M_t/M_∞ is the fraction of drug released over the time t, K a constant dependent on the system, and n is the diffusional exponent, describing the mechanism of transport of drug through the delivery system[47,48]. In general, with minor adjustments based on the specific characteristics of the systems: (i) for moderately swelling systems, a value of 0.5 indicates Fickian diffusion; (ii) a value $0.5 < n < 1$, indicates non-Fickian or anomalous transport, where the mechanism of drug release is governed by both diffusion and swelling; and (iii) $n > 1$, representing an extreme form of transport, suggests a Super Case II transport mechanism dependent on the relaxation of the polymer chains in the matrix, from a vitreous state to a relaxed state rubber type[46,49].

HPLC analysis

The HPLC analyses were conducted in isocratic conditions, employing Perkin Elmer Series 200 HPLC Systems (PerkinElmer, Waltham, MA, USA), equipped with a micropump, an auto sampler, and an UV detector. Particularly, a stainless-steel C-18 reverse-phase column (15×0.46 cm) packed with 5 µm particles (Hypersil

BDSC18 Thermo Fisher Scientific S.p.A., Milan, Italy) was eluted with a mobile phase constituted of methanol/water 80:20 v/v, using a 1 mL/min flow rate. The injection volume was 5 µL, while retention times of CUR and PIP were 2.3 min and 2.7 min, respectively. Wavelength was 360 nm for CUR and 243 nm and for PIP. In case of jointly loaded drugs, the wavelength was set at 360 nm.

Water uptake study

To gain insight into the drug release mechanism, the swelling behavior of the ISFGs formulations was investigated by determining the water uptake of the precursor via gravimetric immersion method. Briefly, 200 µg (M_0) of ISFG were injected into a 10 mL vial filled with 5 mL of bidistilled water and sealed at 37 ± 1 °C. At predetermined time intervals a period of 26 days, the excess water was removed, using 1 mL plastic syringe (MTD, plunger diameter 2 mm) equipped with a 26-G needle. The weight of the ISFG (Mt) was calculated as the difference between the weight of the vial containing the hydrated ISFG formulation and the pre-measured weight of the empty vial. The removed bidistilled water was then replaced with 5 mL of fresh bidistilled water. The water uptake percentage at each time (W_t) was calculated according to Eq. (1):

$$W_t = \frac{(M_t - M_0)}{M_0} \times 100 \quad (1)$$

W_t was determined six times in independent experiments, calculating the mean values ± s.d, and was plotted against the time to evaluate the swelling profile of the analyzed formulations.

In addition, the water uptake data of the linear portion of the swelling profile (1–8 h) were fitted to second order swelling kinetic model according to Eq. (2):

$$\frac{t}{W_t} = \frac{1}{kW_\infty^2} + \frac{t}{W_\infty} \quad (2)$$

Where W_∞ is the maximum water uptake and $k$is the rate constant[50]. The initial swelling rate was then calculated as the the reciprocal of the y-intercept in the plot of t/$W_t$versus t[50–52].

Ex vivo drug release study

Human skin explants were collected from human abdominoplastic surgery as previously described and processed for drug release study of ISFG[53]. Human tissues were obtained via elective abdominoplasty with donor consent under Pearl IRB approval in accordance with FDA 45 CFR 46.102 and 21 CFR 56.102 regulations (Pearl Pathways. Exemption Determination Submission. IRB Study Number: 21-TENB-101. Study Title: Collection, culture, and distribution of human abdominoplasty skin tissue). Written informed consent was obtained from all subjects or, for subjects under 18 years, from a parent and/or legal guardian. All donors were healthy. No identifying information beyond ethnicity, sex and age were provided.

Full thickness skin was rinsed in phosphate buffer saline without calcium and magnesium (Corning® REF 21–040-CV) containing 1% penicillin streptomycin solution (Corning® REF 30-002-CI). After rinsing, skin was injected with 100 µL of ISFG between the dermal and subcutaneous layers, by using a syringe (tissue injection condition). Centered in the place of injection, a 12 mm biopsy was taken with excess subcutaneous fat trimmed. Biopsy was placed in a 12 mm diameter insert with polycarbonate membrane, pore size 0.4 µm, normal pore density 1×10^8 per cm^2 (Costar® REF 3401), and subsequently placed in a 12-well plate with 1 mL of 4.5 g/L glucose Dulbecco's Modified Eagle's Medium (DMEM) (Corning® REF 10–017-CV) supplemented with 10% fetal bovine serum and 1% penicillin streptomycin solution (Fig. S1A-C). After 24 h, samples of culture media, representing the receiving phase, were filtered through nylon syringe filters (0.22 µm) and analyzed by UV for CUR and PIP content, evaluating absorbance at 425 nm and 243 nm wavelengths respectively, using DeNovix DS-11 + Spectrophotometer—UV-Vis Program. Images of ISFGs were taken with DermaLab® Series SkinLab Combo Videoscope probe.

Alternatively, 100 µL of ISFG were directly injected inside the 12-well plate containing the culture media (medium injection condition). After 24 h, the receiving phase was analyzed by UV, as above reported.

Results

Formulative study

A formulative study was conducted to obtain a formulation for a subcutaneous administration of CUR and PIP. The formulation had to be low viscous before the administration to be injectable, while gaining consistency in the subcutaneous site in contact with biological fluids, to obtain a semisolid form, from which the loaded drugs could be release in a sustained manner. GMO and PC were selected as components of ISFG lipid matrix, due to their biocompatibility, biodegradability and extensively studied lyotropic liquid crystals phase behavior. Ethanol was employed as solvent, its presence ensures a homogeneous mixing of the lipid components during the preparation, while regulating the consistency and phase transition properties of the system. In addition, ethanol presence allows to control the ISFG physical stability under storage, preventing bacterial growth[41]. Notably, the lowest possible ethanol amount was employed, to assure biocompatibility and absence of irritative reaction under subcutaneous administration. The acronyms and compositions of ISFGs are reported in Tables 1 and 2. Four different GMO/PC weight ratios were tested, namely 8:2, 7:3, 6:4 and 5:5, w/w, or the sole GMO was explored. For each GMO/PC ratio, the effect of ethanol amount on the syringeability of the system was evaluated.

In the case of GMO (a) and (b), the absence of PC led to the formation of too stiff and not injectable forms, requiring an excipient to modulate the firmness of the system. Conversely, the addition of PC 16–29%, w/w, (GMO/PC weight ratio 7:3 and 8:2) led to softer homogenous mixtures, syringeable in the case of ethanol

ISFG formulations	GMO[1] % w/w	PC[2] % w/w	Ethanol % w/w	Syringeability
GMO (a)	83.5	-	16.5	X
GMO (b)	86.4	-	13.6	X
GMO/PC 8:2 (a)	66.8	16.7	16.5	⎫
GMO/PC 8:2 (b)	69.1	17.3	13.6	X
GMO/PC 8:2 (c)	71.5	17.9	10.6	X
GMO/PC 8:2 (d)	74.1	18.6	7.3	X
GMO/PC 8:2 (e)	77	19.2	3.8	X
GMO/PC 7:3 (a)	58.4	25.1	16.5	⎫
GMO/PC 7:3 (b)	60.4	26	13.6	X
GMO/PC 7:3 (c)	62.6	26.8	10.6	X
GMO/PC 7:3 (d)	64.9	27.8	7.3	X
GMO/PC 7:3 (e)	67.3	28.9	3.8	X
GMO/PC 6:4 (a)	50.1	33.4	16.5	⎫
GMO/PC 6:4 (b)	51.8	34.6	13.6	⎫
GMO/PC 6:4 (c)	53.6	35.8	10.6	X
GMO/PC 6:4 (d)	55.6	37.1	7.3	X
GMO/PC 6:4 (e)	57.7	38.5	3.8	X
GMO/PC 5:5 (a)	41.7	41.7	16.5	⎫
GMO/PC 5:5 (b)	43.2	43.2	13.6	⎫
GMO/PC 5:5 (c)	44.7	44.7	10.6	X
GMO/PC 5:5 (d)	46.3	46.3	7.3	X
GMO/PC 5:5 (e)	48.1	48.1	3.8	X

Table 1. Composition of ISFG and related syringeability. [1]: glyceryl monooleate; [2]: soy phosphatidylcholine.

ISFG formulations	GMO[1] % w/w	PC[2] % w/w	Ethanol % w/w	CUR[3] % w/w	PIP[4] % w/w	Syringeability
GMO5/PC CUR	51.2	34.2	13.6	1	-	✓
GMO5/PC PIP	51.2	34.2	13.6	-	1	✓
GMO5/PC CUR + PIP	51.2	34.2	13.6	0.5	0.5	✓
GMO4/PC CUR	42.7	42.7	13.6	1	-	✓
GMO4/PC PIP	42.7	42.7	13.6	-	1	✓
GMO4/PC CUR + PIP	42.7	42.7	13.6	0.5	0.5	✓

Table 2. Compositions of loaded ISFGs and related syringeability. [1]: glyceryl monooleate; [2]: soy phosphatidylcholine; [3]: curcumin; [4]: piperine.

concentration 16.5% w/w. Higher PC amounts (33–48%, w/w, GMO/PC weight ratio 6:4 and 5:5) resulted in clear and homogeneous mixtures, that were easily syringeable in the case of ethanol 13.6 and 16.5% w/w (Fig. 1A).

The behavior of the syringeable forms in contact with aqueous fluids was considered under injection into bidistilled water at 37 °C. GMO/PC 6:4 and GMO/PC 5:5 (both a and b type) lost their liquid-like behavior immediately after the injection, forming a spherical semi-solid form, minimizing the contact surface with water, as shown in Fig. 1B, suggesting a sol-gel transition due to liquid crystal phase rearrangement.

The spherical gel-like forms maintained in bidistilled water up to 1 month, revealed no macroscopically relevant dissolution phenomena, while a gradual decrease of their transparency was observed (Fig. 1C), probably due to the progressive hydration of the inner core of the systems.

On the other hand, GMO/PC 8:2 (a) and GMO/PC 7:3 (a) underwent a scarce increase of their consistency upon injection in bidistilled water, giving rise to irregular shaped filaments, suggesting a poor suitability as long-lasting delivery systems by subcutaneous injection.

Therefore, GMO/PC 6:4 (b) and GMO/PC 5:5 (b) (hereafter referred to as GMO5/PC and GMO4/PC respectively), based on a lower amount of ethanol with respect to the (a) counterparts (Table 1), were selected for drug loading.

CUR and PIP were thus solubilized in selected ISFG either separately (CUR or PIP 10 mg/g) or jointly (CUR 5 mg/g + PIP 5 mg/g). The ISFGs compositions are reported in Table 2.

Structural characterization and phase transition

The structural characterization of the different samples, both considered as empty and drug loaded formulations, has been performed by X-ray scattering techniques. SAXS was used to investigate the pre-hydrated samples,

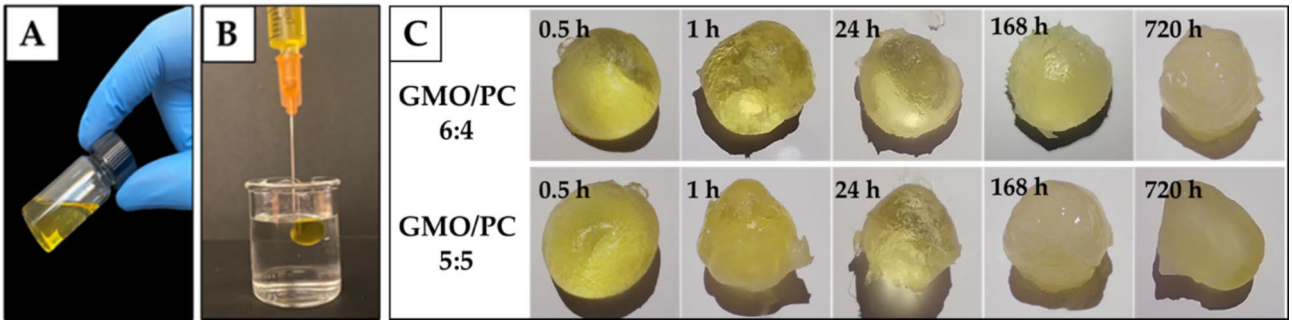

Fig. 1. Representative pictures of GMO 6:4 (b) and GMO 5:5 (b), before (**A**) and after (**B**) injection in bidistilled water; and representative pictures of related structures after different hydration times, up to 30 days (**C**).

while XRD for the post-hydration samples. All the SAXS profiles, reported in Fig. 2 (A for GMO4/PC, and B for GMO5/PC), show a broad band centred at the Q position of about 0.19 $Å^{-1}$, which corresponds to a repeat distance of about 33 Å. The very large band suggest the presence of a disordered inverted micellar phase (in the GMO phase diagram, this phase is indicated as "fluid isotropic"[54]. Two points can be underlined. First, the profile does not change even in the presence of drugs. Second, the WAXS profiles (see Fig. S2) do not present diffraction peaks, but only a broad band around 4.5 Å, related to the liquid-like conformation of the lipid chains, suggesting that the drugs are completely dispersed in the micellar phase. Samples are then homogeneous and disordered.

Conversely, the scattering profiles of the hydrated gel form of GMO/PC formulations are characterized by a series of Bragg peaks (see Fig. 2C-E-G and D-F-H), indicating that the lipid matrix is rather ordered. According to the peak indexation (see black vertical lines), the formation of a hexagonal phase, eventually existing in the presence of a cubic *Pn3m*phase, can be suggested[55]. Indeed, the phase behavior of the GMO/PC gel-like system depends on water composition, c_w, and equilibration time.

Figure 2C and D illustrate the phase behavior of GMO4/PC and GMO5/PC, stabilized for 2 weeks at different water compositions (0.3, 0.4, 0.5 and in the excess of water). In both cases a hexagonal (H) structure forms: the H phase occurs as a single phase in the excess of water, and in combination with a second phase (unidentifiable since only a low intensity peak is detected) in the conditions of lower water composition. The hexagonal unit cell (which corresponds to the distance between the water cylindrical micelles packed in the 2-D hexagonal lattice) is around 72.5 Å for GMO4/PC at all the investigated water compositions and around 65.9 Å for GMO5/PC. In this case, the secondary peak reduces and moves to larger Q when the water composition increases. Such results indicate that the investigated GMO/PC formulations preferentially form hexagonal structures, more swelled when the PC content is larger; the presence of other types of structural organizations, confirmed by the presence of the secondary peaks, suggests that at low water composition, samples need longer equilibration times. Indeed, Fig. 2E and F return to this point: the reported XRD profiles confirm that GMO4/PC prepared in the excess of water show a fair amount of homogeneity already after 48 h equilibration time, while GMO5/PC becomes homogeneous more slowly. For GMO5/PC, noteworthy is the presence of two peaks or one peak and a clearly visible shoulder (Fig. 2D, first and second profile from the bottom), the position of which can be indexed with the first 2 peaks of a cubic *Pn3m* phase. If this identification is correct, the peaks related to the cubic phase, centred in fixed positions which correspond to a unit cell of about 80 Å, disappear at increasing times, while the cell size of the hexagonal phase increases, due to swelling, up to the final value of 65.9 Å.

The last panel of Fig. 2 (2G and 2 H) shows a comparison of the XRD profiles obtained from a series of gel-like formulations, empty and loaded with CUR, PIP and CUR plus PIP, prepared in the excess of water and equilibrated for 48 h. All profiles indicate the formation of ordered structures, mainly of hexagonal type. For GMO4/PC loaded with CUR, PIP or both CUR and PIP, the hexagonal phase (with unit cells of about 73 Å) occurs in the presence of a second phase, which cannot be identified as only one low-intensity peak is detected. According to the GMO phase diagram, the peak could correspond to a lamellar phase (with unit cell around 46–48Å) or to a low water concentration hexagonal phase (unit cell of about 53–55 Å). Note that after 2 weeks only the hexagonal phase with unit cells of about 73 Å remains (data not shown). The GMO5/PC sample shows a similar 2-phase organization: the peak indexing confirms the presence of the hexagonal phase with unit cell around 65.9 Å and of a cubic phase *Pn3m* symmetry (unit cell around 80 Å). Noticeable is the fact that the presence of PIP and/or CUR does not affect at all the structural organization of the gel-like. As before, after 2 weeks of equilibration, only the hexagonal phase with unit cells of 65.9 Å remains (data not shown). This is an important feature that demonstrates the possibility of using such gel-like systems as ISFG.

In vitro release

To investigate the capability of ISFG to control the release of the loaded drugs, the release profile of CUR and/or PIP from GMO5/PC and GMO4/PC were determined in vitro by dialysis method and compared with the ones obtained for free PIP or CUR. At this regard, CUR or PIP ethanol solutions (10 mg/ml) were injected into the dialysis tube, maintaining the same 0.3 v/v vehicle/water ratio employed in the case of ISFG. Due to the different drug solubility, a suspension in the case of CUR, or a solution in the case of PIP were obtained. Ethanol/water

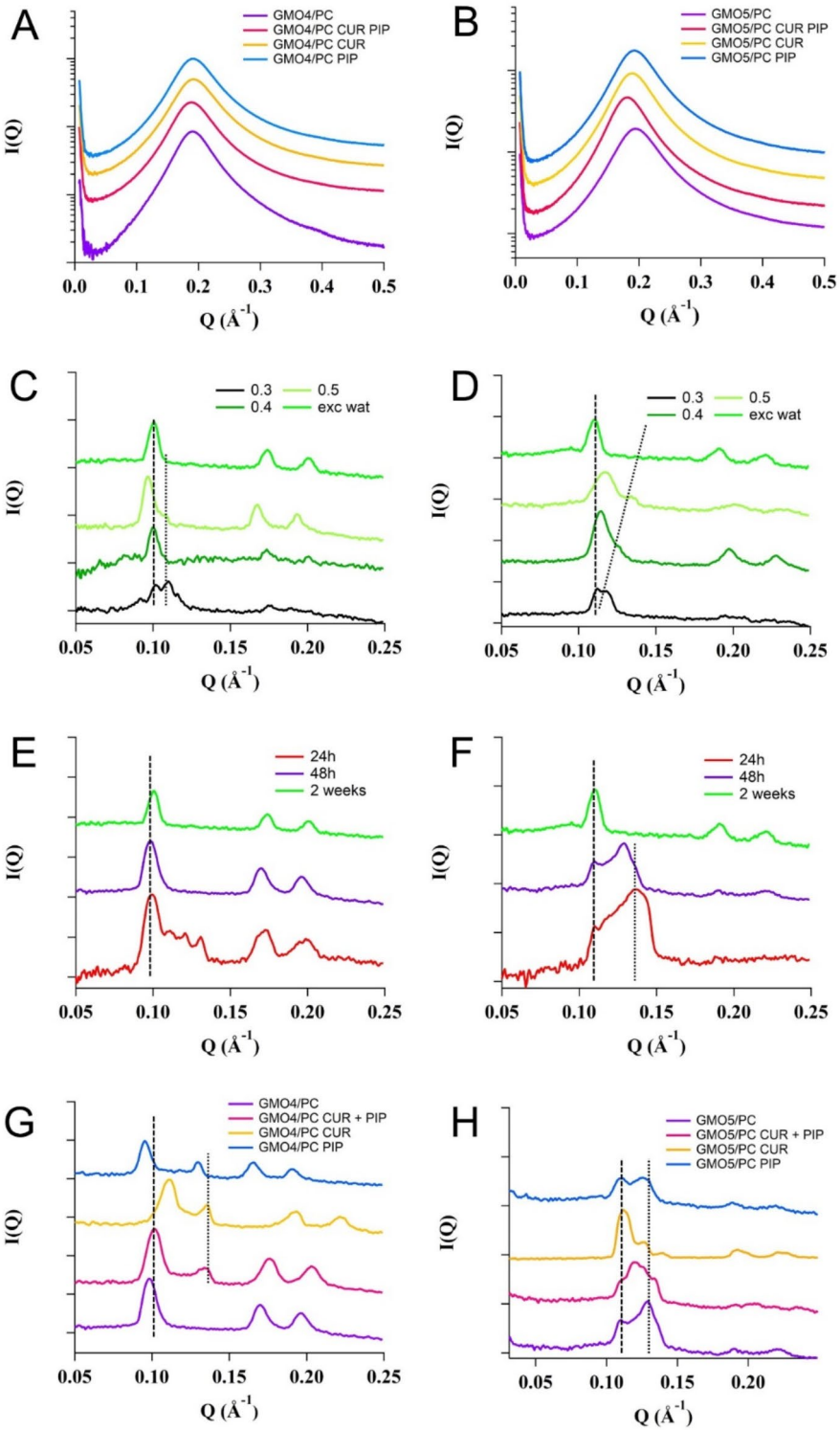

Fig. 2. SAXS (**A**, **B**) and XRD (**C**–**H**) profiles of GMO4/PC (**A**, **C**, **E**,**G**) and GMO5/PC (**B**, **D**, **F**, **H**) formulations pre- (**A**, **B**) and post-hydration (**C**, **D**, **E**, **F**, **G**, **H**). The black vertical lines indicate the position of the main characteristic diffraction peaks for hexagonal phase. C and D panels are related to samples hydrated for two weeks at different water compositions (c_w= 0.3, 0.4, 0.5, and excess of water). E and F panels correspond to the different equilibration times of samples in excess of water. G and H panels refer to samples equilibrated for 48 h, in excess of water.

50:50 (v/v) mixture was employed as receiving phase to guarantee sink conditions. The release profiles, plotted as cumulative % of drug released vs. time, are reported in Fig. 3.

The release kinetics of both CUR and PIP from all ISFG systems exhibited a biphasic profile, characterized by an initial linear drug release phase during the first 8 h, followed by a gradually slower release phase. CUR was released more slowly than PIP, through all formulations, suggesting that CUR was more strongly retained by the lipid matrix, probably due to its higher lipophilicity (logP 3.29) compared to PIP (logP 2.78). The release profiles of both PIP and CUR from the GMO4/PC and GMO5/PC systems were nearly superposable during the initial linear phase (1–8 h), with statistically relevant differences emerging 48 h post-injection. Specifically, the GMO4/PC formulation exhibited a slower release and a total amount of drug release at 96 h lower than the one from GMO5/PC. Notably, the results highlight the capability of both GMO4/PC and GMO5/PC forms to provide a sustained release of CUR and/or PIP up to 96 h after injection. In the case of plain PIP solution, a burst release occurred during the first few hours, followed by a plateau at 24–48 h, while in the case of CUR suspension the release during the first 8 h was superposable to the ones obtained by ISFG, becoming the slowest in the following hours. Remarkably, in the case of jointly loaded formulations faster drug release kinetics, and higher amount of drug released were obtained with respect to the single loaded forms.

To gain insight into the mechanism of CUR and PIP release from ISFGs formulations, the in vitro release profiles were mathematically fitted to several models, namely zero order, first order, Higuchi and Peppas. As reported in Table S1, comparing R^2values, for all the formulations both CUR and PIP release followed first order release kinetics, as found by other authors in the case of lyotropic liquid crystals based self-assembly ISFGs[56–59]. Additionally, the release data for all formulations were well fitted to the Peppas model, with R^2 values consistently above 0.95, allowing its use to evaluate and characterize the influence of swelling and/or erosion phenomena on drug release. The fitting into Peppas equation revealed a non-Fickian diffusion mechanism with release exponent $0.5 < n < 1$, indicating that the drug release was governed by both diffusion and swelling/erosion of the lipid supramolecular structure[60,61].

Water uptake

Considering the results obtained from mechanistic analysis, to shed light into the role and influence of swelling phenomena on drug release kinetic, the swelling behavior of ISFG formulations was evaluated by monitoring their water uptake profiles, reported in Fig. 4A.

As expected, a burst water uptake occurred after the injection into bidistilled water, with water uptake percentages of approximately 20 and 28% for GMO5/PC and GMO4/PC, respectively, 1 h after injection. This behavior is due to the immediate liquid crystalline phase transition (and related sol-gel transition) in the superficial and external regions of the systems, as macroscopically observed during gelation tests and analyzed via SAXS measurements.

The comparison between the water uptake profiles and the release profiles of GMO4/PC and GMO5/PC revealed the key role of swelling in controlling the release kinetics of both CUR and PIP. This observation agrees perfectly with existing literature, which consistently emphasizes the swellable nature of GMO-based gels and their swelling-regulated drug release profile[41,52,59].

In line with the release profiles, the water uptake kinetics of both the formulations were characterized by a biphasic profile, exhibiting an initial rapid and almost linear water uptake increase up to 8/24 h post-injection followed by a gradually slower swelling phase, probably associated with the hydration of the inner part of the systems, reaching the maximum swelling approximately 300 h after injection, with a water uptake at the equilibrium of about 180 and 250% for GMO4/PC and GMO5/PC, respectively.

Furthermore, as previously reported, the release profiles of the formulations during the first 24 h post-injection were nearly superimposable. Similarly, the comparison of the swelling profiles of the two formulations reveals no significant differences up to 24 h.

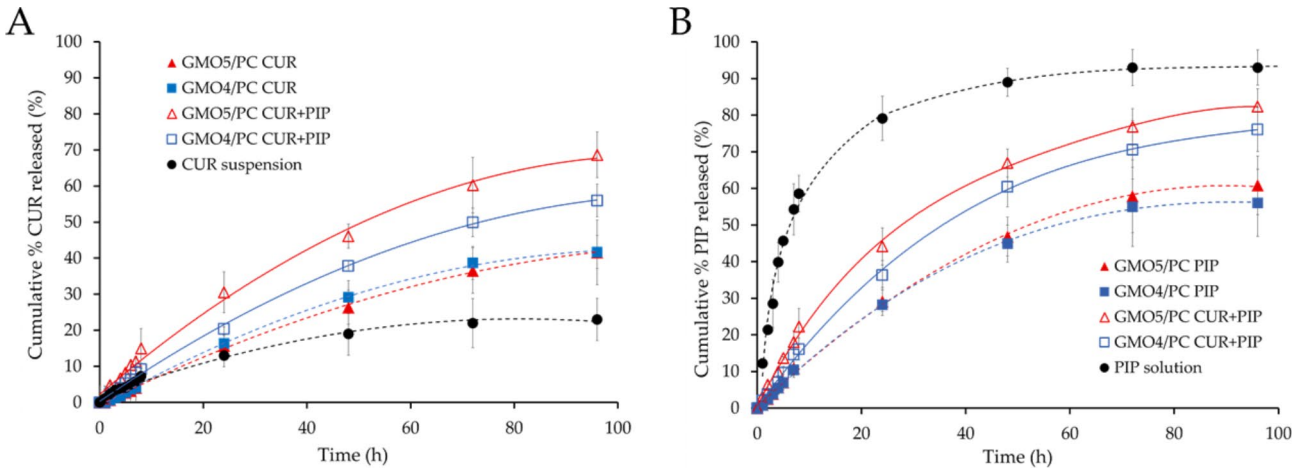

Fig. 3. In vitro release kinetics of CUR (**A**) and PIP (**B**) from ISFG formulations, CUR suspension and PIP solution. Data are the mean of 6 independent experiments ± s.d.

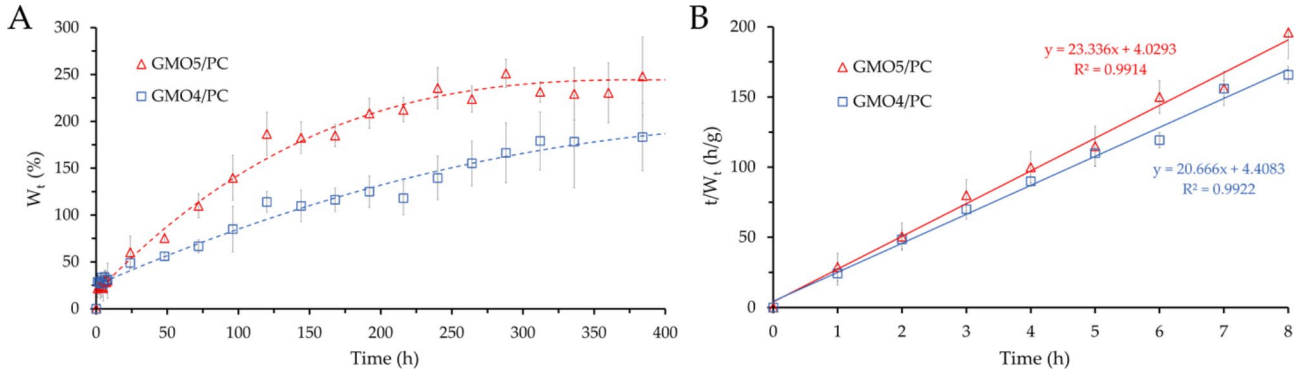

Fig. 4. Water uptake percentage profiles of GMO4/PC and GMO5/PC at 37 ± 1 °C (**A**) and fitting of water uptake data (0–8 h) into second order swelling kinetic equation (**B**). Data are the mean of 6 independent experiments ± s.d.

The water uptake data of the initial linear portion (0–8 h) were also plotted into second order swelling kinetic model (Eq. (2)) (Fig. 4B), to mathematically determine the initial swelling rate of the ISFG formulations, as reported in Sect. 2.7. The initial swelling rate values obtained for GMO5/PC and GMO4/PC, were 0.248 and 0.227 respectively, quantitatively confirming that no significant differences can be detected in the swelling behavior of the two formulations over an 8-h period following injection.

On the other hand, after 48 h from the injection in water, relevant differences in the swelling behavior of GMO4/PC and GMO5/PC were detected.

Considering the results obtained from the in vitro drug release water uptake analyses, GMO5/PC formulation was selected as more suitable formulation for further ex vivo release studies, exhibiting a quantitatively higher and faster release profile compared to GMO4/PC formulation.

Ex vivo drug release study

In order to further investigate the gelation behavior and the drug release processes of the selected formulations in simulated physiological conditions, ex vivo assessments were conducted by using human skin explants[53]. Their injection was simulated in healthy skin biopsies, to investigate the feasibility of the formulations for subcutaneous administration. The formation and the appearance of the gel-like structures in subcutaneous tissues was observed in skin biopsies cross-sections. The obtained images (Fig. 5), confirm the capability of GMO5/PC to undergo sol-gel transition upon absorption of water from physiological subcutaneous environment, obtaining a light yellow transparent semisolid depot system, in agreement with in vitro observations.

As described in Sect. 2.7, ex vivo release analysis was performed to study the release of CUR from GMO5/PC CUR and GMO5/PC CUR + PIP when directly immersed in the culture medium (medium injection condition), or subcutaneously injected in healthy human skin explants, excised by a biopsy punch, and then put in culture medium (tissue injection condition, Fig. S1A-C). In both cases the culture medium constituted the receiving phase.

The medium injection condition was employed to evaluate the direct release of CUR from the ISFG to the receiving phase, while the tissue injection condition was employed to study the processes of CUR release from the GMO5/PC system, followed by CUR diffusion through skin tissues towards the receiving phase. Figure 6 reports the percentage of CUR released in the receiving phase after 24 h, with respect to the total amount of CUR in the formulation.

Due to the experimental conditions, the percentages of CUR released after 24 h were significantly lower with respect to the values obtained by in vitro release analysis. This is clearly related to the very low affinity of CUR for the aqueous culture medium, used as the receiving phase. As expected, the amounts of CUR released from both GMO5/PC CUR and GMO5/PC CUR + PIP formulations under tissue injection condition were lower than the ones obtained under medium injection condition. In the case of medium injection, the percentage of CUR release from GMO5/PC CUR and GMO5/PC CUR + PIP is almost superposable. Conversely, in the case of tissue injection a higher percentage of CUR release was found from GMO5/PC CUR + PIP with respect to GMO5/PC CUR, suggesting that the presence of PIP could increase the release/diffusion of CUR.

Discussion

One of the key advantages of ISFGs over other advanced controlled release systems is their ease of preparation, combined with high stability and storability[40,62]. In the present study, the ISFG precursors were obtained by simply mixing the components under magnetic stirring in a one-step procedure, without the use of any other external high-energy input. Due to their simple one-phase liquid form, the systems enable high entrapment capacity, stability, and storability, effectively preventing phase separation or destabilization phenomena commonly observed in dispersed drug delivery systems. In a recent study we investigated the delivery of CUR and PIP in ethosomes, achieving a final 0.25 mg/ml content of jointed drugs. Noteworthily, the ISFG delivery strategy enabled to 40-fold increase the total loading of the same drugs[32].

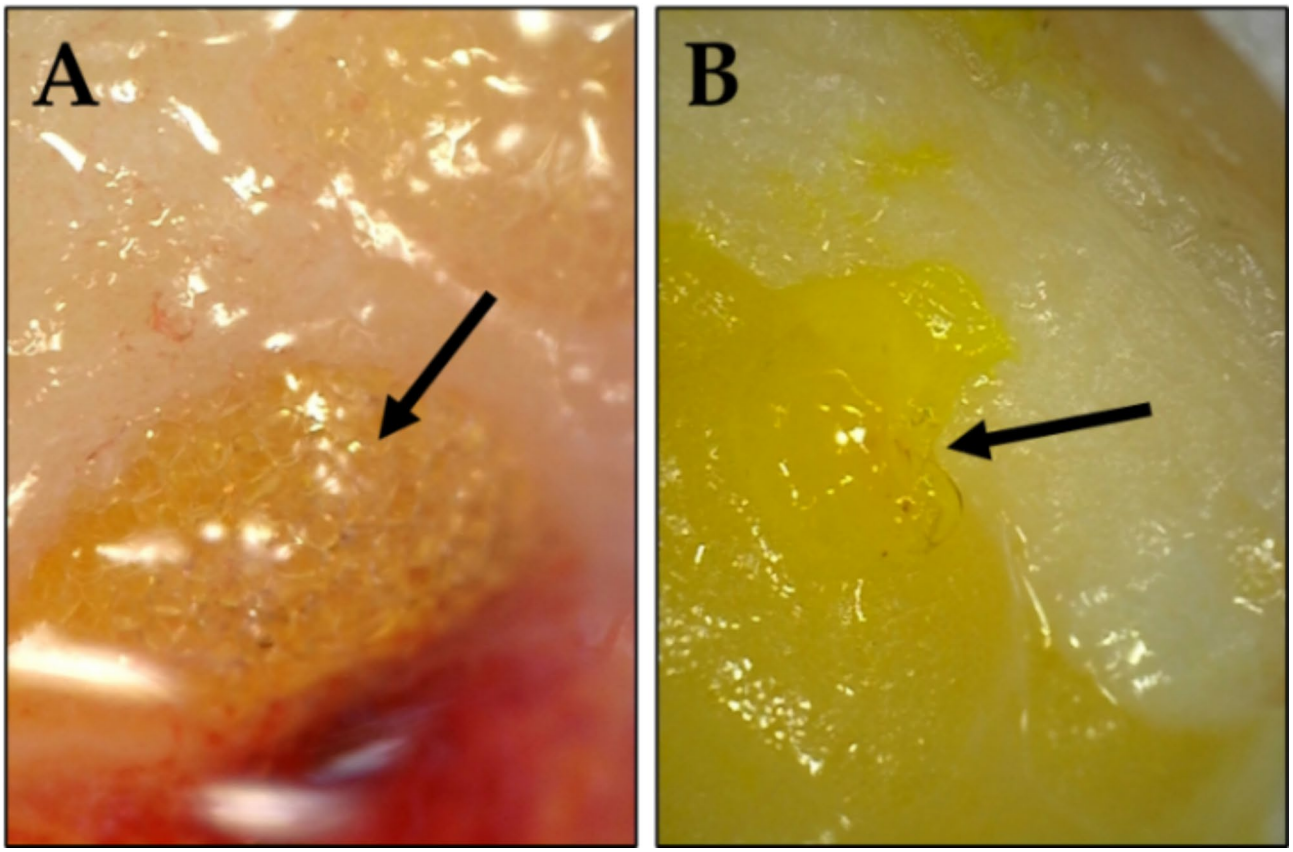

Fig. 5. Cross-section images of healthy human skin explants after GMO5/PC (**A**) and GMO5/PC CUR + PIP subcutaneous injection.

Remarkably, a higher and faster release of both CUR and PIP was observed in the case of jointly loaded GMO4/PC and GMO5/PC, with respect to the separately loaded ones, probably due to a different structural organization of the lipid matrix in the case of the combined presence of drugs, promoting their diffusion, as previously observed[32].

The slower swelling kinetic and lower final water uptake percentage of GMO4/PC with respect to GMO5/PC well agree with the release kinetic results, highlighting a faster and greater release of both drugs from 48 h, for GMO5/PC, with respect to GMO4/PC. It is likely that the higher swelling capability of GMO5/PC could account for the faster drug release with respect to GMO4/PC.

As evidenced by some authors, the dialysis membrane method, employed to in vitro evaluate the drug release from pharmaceutics, in some cases could not give a true description of the drug-release profile, influencing the kinetic, as a function of the membrane cut-off[63,64]. Anyways, drug release studies using the dialysis membrane technique can be appropriate to obtain a qualitative assessment of release from different drug carriers, for comparative studies, as the case of this investigation[65]. Notably, in the present study it should be underlined that the release of the free drugs was completely different from the profiles of the drugs loaded in ISFG, suggesting the suitability of the method. Furthermore, an ex-vivo study was conducted to obtain more reliable information about CUR and PIP release kinetics, achieving interesting results.

Indeed, under medium injection conditions, no significant differences were detected between CUR loaded ISFG and CUR + PIP jointly loaded system. Conversely, under tissue injection conditions, GMO5/PC CUR + PIP demonstrated an almost two-fold higher percentage of CUR released, compared to that obtained for GMO5/PC CUR. Remarkably, this result suggest a CUR release/penetration enhancement effect, related to the presence of PIP. This effect could be attributed to a different structural organization of GMO5/PC CUR + PIP with respect to GMO5/PC CUR, in perfect agreement with the results obtained from the in vitro release tests. Nevertheless, under media injection condition, no significant differences were observed. Therefore, it can be hypothesized that on one hand the presence of PIP enhances CUR release/diffusion due to a structural alteration of the ISFG system, while on the other, in the subcutaneous tissues environment, PIP might exert some influence on the physiological surroundings during release.

Conclusions

The formulative study demonstrated that GMO in the presence of PC and ethanol enabled to obtain ISFG suitable for CUR and PIP loading and subcutaneous administration. After injection in water, a transition from micellar to hexagonal and cubic phase occurred, leading to swellable semisolid forms suitable to sustain CUR

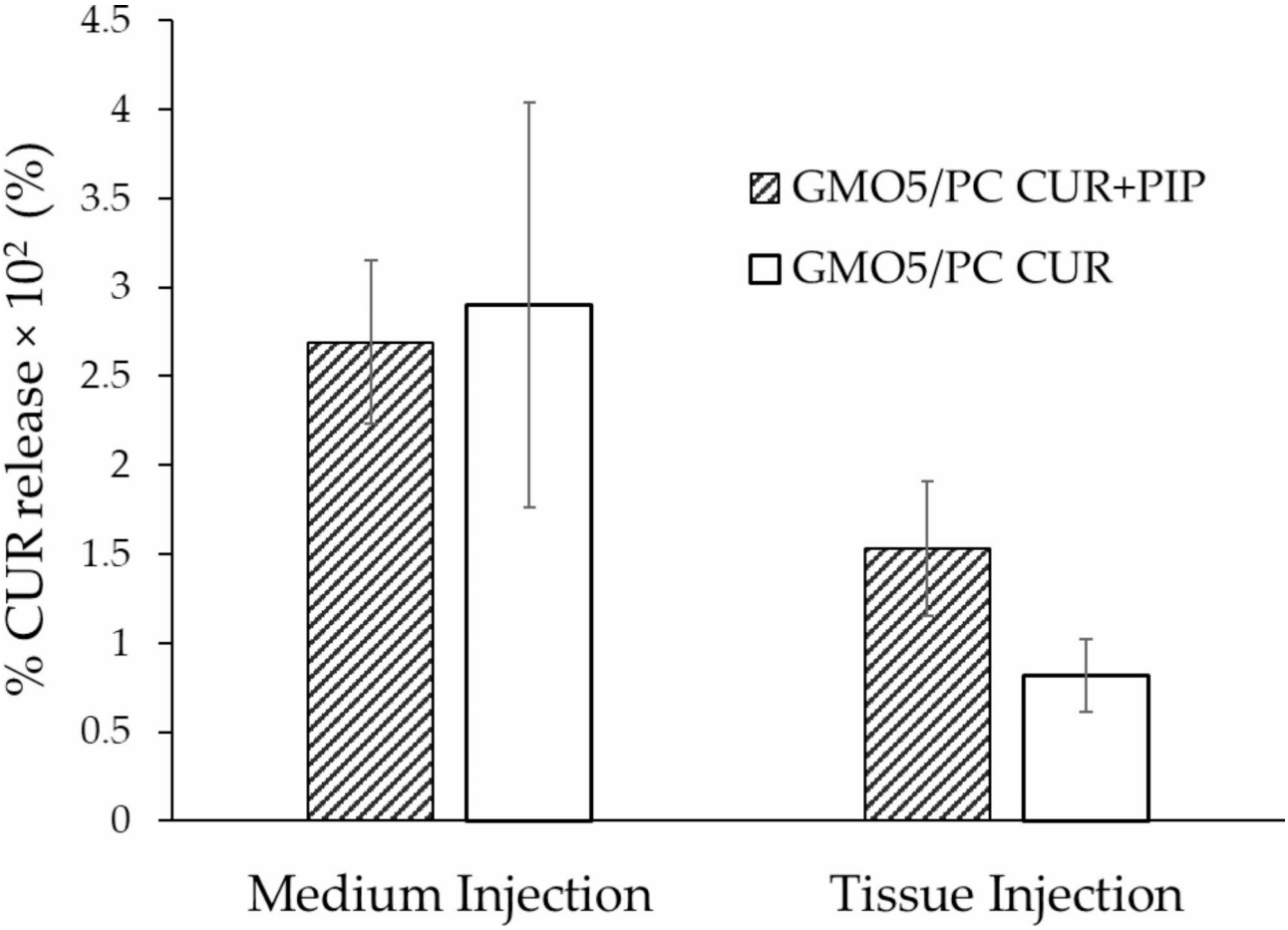

Fig. 6. Ex vivo percentage of CUR released in the receiving phase from GMO5/PC CUR + PIP and GMO5/PC CUR in the two different experimental conditions tested.

and PIP release through 4 days. Both in vitro and ex-vivo studies suggested an increase of CUR release in the case of its co-loading with PIP. However, further in-depth studies are required to better clarify the PIP potential penetration enhancement effect in subcutaneous tissues, as well as the efficacy of ISFG loaded with CUR and PIP in the treatment of inflammatory and degenerative joint diseases.

Data availability

The authors declare that the data supporting the findings of this study are available within the paper and its Supplementary Information files. Should any raw data files be needed in another format they are available from the corresponding author upon reasonable request.

Received: 4 November 2024; Accepted: 21 January 2025
Published online: 24 January 2025

References

1. 1. Chin, K. Y. The spice for joint inflammation: Anti-inflammatory role of curcumin in treating osteoarthritis. *Drug Des. Dev. Ther.* **10** (2016).
2. 2. Taylor, S. & Lobo, A. J. Diagnosis and treatment of inflammatory bowel disease. in *Practitioner* **260** (2016).
3. 3. Ledingham, J., Snowden, N. & Ide, Z. Diagnosis and early management of inflammatory arthritis. *BMJ* **358**, (2017).
4. 4. Almutairi, K., Nossent, J., Preen, D., Keen, H. & Inderjeeth, C. The global prevalence of rheumatoid arthritis: A meta-analysis based on a systematic review. *Rheumatol. Int.* **41**, (2021).
5. 5. Brown, P., Pratt, A. G. & Hyrich, K. L. Therapeutic advances in rheumatoid arthritis. *BMJ* (2024) 10.1136/bmj-2022-070856.
6. 6. Aletaha, D. *et al.* Rheumatoid arthritis classification criteria: An American College of Rheumatology/European League Against Rheumatism collaborative initiative. *Ann. Rheum. Dis.* **69** (2010).
7. 7. Lin, Y. J., Anzaghe, M. & Schülke, S. Update on the pathomechanism, diagnosis, and treatment options for rheumatoid arthritis. *Cells* **9** (2020).
8. 8. Simons, G. *et al.* Systematic review of quantitative preference studies of treatments for rheumatoid arthritis among patients and at-risk populations. *Arthritis Res. Ther.* **24** (2022).
9. 9. Radu, A. F. & Bungau, S. G. Nanomedical approaches in the realm of rheumatoid arthritis. *Ageing Res. Rev.* **87** (2023).
10. 10. Babaahmadi, M. *et al.* Rheumatoid arthritis: the old issue, the new therapeutic approach. *Stem Cell Res. Ther.* **14** (2023).
11. 11. Burmester, G. R. & Pope, J. E. Novel treatment strategies in rheumatoid arthritis. *The Lancet* **389** (2017).

12. 12. Zhao, J. H. *et al.* Clinically approved small-molecule drugs for the treatment of rheumatoid arthritis. *Eur. J. Med. Chem.* **256** (2023).
13. 13. Fraenkel, L. *et al.* 2021 American college of rheumatology guideline for the treatment of rheumatoid arthritis. *Arthritis Care Res.* **73**, (2021).
14. 14. Negrei, C. *et al.* Management of rheumatoid arthritis: Impact and risks of various therapeutic approaches (Review). *Experimental and Therapeutic Medicine* **11** (2016).
15. 15. Singh, J. A. *et al.* Risk of serious infection in biological treatment of patients with rheumatoid arthritis: A systematic review and meta-analysis. *Lancet* **386**, (2015).
16. 16. Avouac, J. & Allanoret, Y. Cardiovascular risk in rheumatoid arthritis: Effects of anti-TNF drugs. *Expert Opinion on Pharmacotherapy* **9** (2008).
17. 17. Raksasuk, S. & Ungprasert, P. Patients with rheumatoid arthritis have an increased risk of incident chronic kidney disease: A systematic review and meta-analysis of cohort studies. *International Urology and Nephrology***52** (2020).
18. 18. Hewlings, S. J. & Kalman, D. S. Curcumin: A review of its effects on human health. *Foods* **6** (2017).
19. 19. Gupta, S. C., Patchva, S., Koh, W. & Aggarwal, B. B. Discovery of curcumin, a component of golden spice, and its miraculous biological activities. *Clin. Exp. Pharmacol. Physiol.* **39**, (2012).
20. 20. Zheng, D. *et al.* Antibacterial mechanism of curcumin: A review. *Chemi. Biodiv.* **17** (2020).
21. 21. Mohammadian Haftcheshmeh, S. *et al.* Immunomodulatory effects of curcumin in rheumatoid arthritis: Evidence from molecular mechanisms to clinical outcomes. in *Rev. Physiol. Biochem. Pharmacol.* **179** (2021).
22. 22. Kou, H. *et al.* Effect of curcumin on rheumatoid arthritis: A systematic review and meta-analysis. *Frontiers in Immunology* **14** (2023).
23. 23. Makuch, S., Więcek, K. & Woźniak, M. The immunomodulatory and anti-inflammatory effect of curcumin on immune cell populations, cytokines, and in vivo models of rheumatoid arthritis. *Pharmaceuticals* **14**, (2021).
24. 24. Pourhabibi-Zarandi, F., Shojaei-Zarghani, S. & Rafraf, M. Curcumin and rheumatoid arthritis: A systematic review of literature. *Int. J. Clin. Pract.* **75** (2021).
25. 25. Haq, I. U. *et al.* Piperine: A review of its biological effects. *Phytotherapy Res.* **35** (2021).
26. 26. Tripathi, A. K., Ray, A. K. & Mishra, S. K. Molecular and pharmacological aspects of piperine as a potential molecule for disease prevention and management: Evidence from clinical trials. *Beni-Suef University Journal of Basic and Applied Sciences* vol. 11 (2022).
27. 27. Bang, J. S. *et al.* Anti-inflammatory and antiarthritic effects of piperine in human interleukin 1β-stimulated fibroblast-like synoviocytes and in rat arthritis models. *Arthritis Res. Ther.* **11**, (2009).
28. 28. Bhalekar, M. R., Madgulkar, A. R., Desale, P. S. & Marium, G. Formulation of piperine solid lipid nanoparticles (SLN) for treatment of rheumatoid arthritis. *Drug Dev. Ind. Pharm.* **43**, (2017).
29. 29. Kesarwani, K. & Gupta, R. Bioavailability enhancers of herbal origin: An overview. *Asian Pac. J. Trop. Biomed.* **3**, (2013).
30. 30. Moorthi, C. & Kathiresan, K. Curcumin-piperine/curcumin-quercetin/curcumin- silibinin dual drug-loaded nanoparticulate combination therapy: A novel approach to target and treat multidrug-resistant cancers. *J. Med. Hypotheses Ideas* **7**, (2013).
31. 31. Jantarat, C., Sirathanarun, P., Boonmee, S., Meechoosin, W. & Wangpittaya, H. Effect of piperine on skin permeation of curcumin from a bacterially derived cellulose-composite double-layer membrane for transdermal curcumin delivery. *Sci. Pharm.* **86**, (2018).
32. 32. Ferrara, F. *et al.* Ethosomes for curcumin and piperine cutaneous delivery to prevent environmental-stressor-induced skin damage. *Antioxidants* **13**, (2024).
33. 33. Prasad, S., Tyagi, A. K. & Aggarwal, B. B. Recent developments in delivery, bioavailability, absorption and metabolism of curcumin: The golden pigment from golden spice. *Cancer Res. Treatment* **46** (2014).
34. 34. Zhang, W. *et al.* A review on the bioavailability, bio-efficacies and novel delivery systems for piperine. *Food and Function* **12** (2021).
35. 35. An, X. *et al.* Advances in local drug delivery technologies for improved rheumatoid arthritis therapy. *Adv. Drug Deliv. Rev.* **209**, 115325 (2024).
36. 36. Li, B. *et al.* Injectable "nano-micron" combined gene-hydrogel microspheres for local treatment of osteoarthritis. *NPG Asia Mater.* **14**, (2022).
37. 37. Gagliardi, A. *et al.* Design and characterization of glyceryl monooleate-nanostructures containing doxorubicin hydrochloride. *Pharmaceutics* **12**, (2020).
38. 38. Kulkarni, C. V., Wachter, W., Iglesias-Salto, G., Engelskirchen, S. & Ahualli, S. Monoolein: A magic lipid? *Physical Chemistry Chemical Physics* **13** (2011).
39. 39. Milak, S. & Zimmer, A. Glycerol monooleate liquid crystalline phases used in drug delivery systems. *International Journal of Pharmaceutics* **478** (2015).
40. 40. Kempe, S. & Mäder, K. In situ forming implants - An attractive formulation principle for parenteral depot formulations. *Journal of Controlled Release* **161** (2012).
41. 41. Mei, L. *et al.* Injectable in situ forming gel based on lyotropic liquid crystal for persistent postoperative analgesia. *Acta Biomater.* **67**, (2018).
42. 42. Das, T., Prakash, V. M. & Math, P. K. T. Injectable in situ gel of methotrexate for rheumatoid arthritis: Development, in vitro and in vivo evaluation. *J. Appl. Pharm. Sci.* **9**, (2019).
43. 43. Striesow, F. & Brandt, A. Preference, satisfaction and usability of subcutaneously administered methotrexate for rheumatoid arthritis or psoriatic arthritis: Results of a postmarketing surveillance study with a high-concentration formulation. *Ther. Adv. Musculoskelet. Dis.* **4**, (2012).
44. 44. Yin, N. *et al.* Intra-articular injection of indomethacin-methotrexate: In situ hydrogel for the synergistic treatment of rheumatoid arthritis. *J. Mater. Chem. B* **8**, (2020).
45. 45. Amenitsch, H., Bernstorff, S. & Laggner, P. High-flux beamline for small-angle x-ray scattering at ELETTRA. *Rev. Sci. Instrum.* **66**, (1995).
46. 46. Mathematical models of drug release. in *Strategies to Modify the Drug Release from Pharmaceutical Systems* (2015). doi:10.1016/b978-0-08-100092-2.00005-9.
47. 47. Peppas, N. A. & Sahlin, J. J. A simple equation for the description of solute release. III. Coupling of diffusion and relaxation. *Int. J. Pharm.* **57**, (1989).
48. 48. Ritger, P. L. & Peppas, N. A. A simple equation for description of solute release II. Fickian and anomalous release from swellable devices. *J. Control. Release* **5**, (1987).
49. 49. Dash, S., Murthy, P. N., Nath, L. & Chowdhury, P. Kinetic modeling on drug release from controlled drug delivery systems. *Acta Poloniae Pharmaceutica - Drug Research* **67** (2010).
50. 50. Schott, H. Kinetics of swelling of polymers and their gels. *J. Pharm. Sci.* **81**, (1992).
51. 51. Ofner, C. M. & Schott, H. Swelling studies of gelatin I: Gelatin without additives. *J. Pharm. Sci.* **75**, (1986).
52. 52. Lee, J., Choi, S. U., Yoon, M. K. & Young, W. C. Kinetic characterization of swelling of liquid crystalline phases of glyceryl monooleate. *Arch. Pharm. Res.* **26**, (2003).
53. 53. Ivarsson, J. *et al.* Comparison of pollutant effects on cutaneous inflammasomes activation. *Int. J. Mol. Sci.* **24**, (2023).
54. 54. Mazzoni, S., Barbosa, L. R. S., Funari, S. S., Itri, R. & Mariani, P. Cytochrome-c affects the monoolein polymorphism: consequences for stability and loading efficiency of drug delivery systems. *Langmuir* **32**, (2016).

55. 55. Esposito, E., Mariani, P., Drechsler, M. & Cortesi, R. Structural studies of lipid-based nanosystems for drug delivery: X-ray diffraction (XRD) and cryogenic transmission electron microscopy (Cryo-TEM). in *Handbook of Nanoparticles* (2015). doi:10.1007/978-3-319-15338-4_39.
56. 56. Wang, B. *et al.* Self-assembling in situ gel based on lyotropic liquid crystals containing VEGF for tissue regeneration. *Acta Biomater.* **99**, (2019).
57. 57. Huang, Y. & Gui, S. Factors affecting the structure of lyotropic liquid crystals and the correlation between structure and drug diffusion. *RSC Advances* **8** (2018).
58. 58. Lara, M. G., Bentley, M. V. L. B. & Collett, J. H. In vitro drug release mechanism and drug loading studies of cubic phase gels. *Int. J. Pharm.* **293**, (2005).
59. 59. Rizwan, S. B., Hanley, T., Boyd, B. J., Rades, T. & Hook, S. Liquid crystalline systems of phytantriol and glyceryl monooleate containing a hydrophilic protein: Characterisation, swelling and release kinetics. *J. Pharm. Sci.* **98**, (2009).
60. 60. Mircioiu, C. *et al.* Mathematical modeling of release kinetics from supramolecular drug delivery systems. *Pharmaceutics* **11** (2019).
61. 61. Talevi, A. & Ruiz, M. E. Korsmeyer-Peppas, Peppas-Sahlin, and Brazel-Peppas: Models of drug release. in *The ADME Encyclopedia* (2021). 10.1007/978-3-030-51519-5_35-1.
62. 62. Ruel-Gariépy, E. & Leroux, J. C. In situ-forming hydrogels - Review of temperature-sensitive systems. *European Journal of Pharmaceutics and Biopharmaceutics* **58** (2004).
63. 63. Yu, M., Yuan, W., Li, D., Schwendeman, A. & Schwendeman, S. P. Predicting drug release kinetics from nanocarriers inside dialysis bags. *J. Control. Release* **315**, (2019).
64. 64. Zambito, Y., Pedreschi, E. & Di Colo, G. Is dialysis a reliable method for studying drug release from nanoparticulate systems? - A case study. *Int. J. Pharm.* **434**, (2012).
65. 65. Moreno-Bautista, G. & Tam, K. C. Evaluation of dialysis membrane process for quantifying the in vitro drug-release from colloidal drug carriers. *Colloids Surfaces A Physicochem. Eng. Asp.* **389**, (2011).

Acknowledgements

The authors disclose support for the research of this work from Funders PRIN 2022 (2022MC2SKF), Italian Ministry of University and Research, European Union, Next Generation EU, and FAR 2023, University of Ferrara, Italy.

Author contributions

E.E., W.P. F.F and G.V. wrote the main manuscript text. W.P., A.B., F.F., P.M., A.P. and M.G.O. wrote the methods section and results. W.P. prepared Figs. 1 and 3, and 4. A.P., P.M. and M.G.O. prepared Fig. 2. F.F., A.P. and J.I. prepared Figs. 5 and 6. All authors reviewed the manuscript.

Funding

This research was funded by PRIN 2022 (2022MC2SKF), Italian Ministry of University and Research, European Union, Next Generation EU, and FAR 2023, University of Ferrara, Italy.

Declarations

Competing interests

The authors declare no competing interests.

Additional information

Supplementary Information The online version contains supplementary material available at https://doi.org/10.1038/s41598-025-87750-w.

Correspondence and requests for materials should be addressed to G.V. or E.E.